Energetics and Mechanism for the Deamination of Lithiated Cysteine

P. B. Armentrout,* Sha Joshua Ye, Amy Gabriel, and R. M. Moision

Department of Chemistry, University of Utah, 315 S. 1400 E. Rm 2020, Salt Lake City, Utah 84112

Received: November 25, 2009; Revised Manuscript Received: February 9, 2010

Lithium cation complexes with cysteine (Cys) are collisionally activated with xenon in a guided ion beam tandem mass spectrometer and observed to deaminate in addition to loss of the intact amino acid. Source conditions are found to influence the cross sections for these processes considerably, a result interpreted in terms of two isomers, Li^+(Cys) and $(NH_3)Li^+(C_3H_4O_2S)$. Quantum chemical calculations at the B3LYP/6-311G(d,p) level are used to explore the reaction mechanism for this fragmentation process in detail. A complete reaction coordinate surface for the process is elucidated, including all intermediates and transition states. Theoretical molecular parameters for the two isomers and for the rate-limiting transition state for deamination of Li^+(Cys) are then used to analyze the threshold energies in the experimental data, providing experimental measurements of the energies of the transition state and various products. These experimental energies are compared with single point energies calculated at three different levels, B3LYP, B3P86, and MP2(full), using the 6-311+G(2d,2p) basis set with geometries and zero point energies calculated at the B3LYP/6-311G(d,p) level, as well as with additional calculations using basis sets that include core correlation on lithium. Good agreement between experiment and theory suggests that the reaction mechanisms have been reasonably elucidated and identifies the $C_3H_4O_2S$ deamination product as thiirane-carboxylic acid.

Introduction

In the previous paper (part I, DOI 10.1021/jp911219u),[1] we examine the intrinsic properties of the pairwise interaction of alkali metal cations (Li^+, Na^+, K^+, and Rb^+) with the amino acid cysteine (Cys) by measuring the threshold collision-induced dissociation (TCID) of the M^+(Cys) complexes in a guided ion beam tandem mass spectrometer. For the sodiated, potassiated, and rubidiated complexes, only loss of the intact amino acid is observed, thereby allowing straightforward interpretation of the threshold for this process in terms of the bond dissociation energy between the metal cation and cysteine. In the case of the lithiated complex, loss of the intact ligand is the entropically favored process at high energies, but because the binding energy of lithium cations to cysteine is comparable to covalent bond energies within Cys, an additional decomposition reaction is observed at lower collision energies. This process occurs not only upon collisional activation but also during association of Li^+ with Cys in the source region, such that the data acquired for the lithium system is composed of two isomers, hypothesized to be Li^+(Cys) and $(NH_3)Li^+(C_3H_4O_2S)$, which need to be carefully deconvoluted. To fully understand this process, to identify the deamination product, and to meaningfully interpret the threshold energies, knowledge of the rate-limiting transition state is needed, which in turn requires information about the potential energy surface for these reactions. The complexity of these processes necessitates a detailed examination of a number of potential pathways, which is the focus of this paper. The $C_3H_4O_2S$ deamination products considered include 3-mercaptopropenoic acid (Mpa), thioacetaldehyde-2-carboxylic acid (Taca), the three-membered ring thiirane-carboxylic acid (Tica), and 3-mercapto-α-propiolactone (Mpl), Scheme 1. Ultimately, the theoretical energies of the calculated rate-limiting transition states can be compared to the experimental thresholds, thereby providing a means of testing whether the appropriate reaction mechanism has been located and identifying the fragments formed.

SCHEME 1

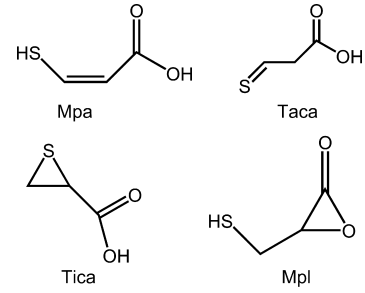

It can be recognized that the elucidation of such fragmentation processes is not only of fundamental interest but may also prove useful in understanding decomposition reactions observed in analytical mass spectrometry experiments that are designed to probe the sequence of peptides and proteins.[2−9] As the decomposition of the side chain can compete with backbone cleavages that give sequence information, a quantitative characterization of such decompositions may prove useful in interpreting such analytical experiments.

Experimental and Computational Section

General Experimental Procedures. The GIBMS used to measure the cross sections for TCID of the alkali metal cation Cys complexes has been described previously in detail,[10,11] as outlined briefly in part I (DOI 10.1021/jp911219u) for the present system. Here, the ions of interest are formed in a dc discharge flow tube (DC/FT) source.[12] Lithium cations are generated at the cathode, a tantalum boat filled with lithium located at the head of a 1 m long flow tube, by using a continuous dc discharge with typical operating conditions of

10.1021/jp911222j
Published on Web 02/25/2010

1.9−2.2 kV and 10−20 mA. The lithium cations are carried down the flow tube by a buffer gas (ca. 10% argon in helium) with normal operating pressures of 0.3−0.4 Torr. About 50 cm downstream from the discharge, cysteine is introduced into the flow tube using a temperature controlled probe, which is heated to either ∼120 or ∼180 °C. Complexes of interest are formed via three-body associative reactions of lithium with Cys in the flow of the He/Ar carrier gas. The complex ions are thermalized to 300 K (the temperature of the flow tube) both vibrationally and rotationally by undergoing $\sim 10^5$ collisions with the buffer gases as they drift along the 1 m long flow tube.[12−19]

Data Analysis. The preceding paper[1] (DOI 10.1021/jp911219u) discusses the means used to analyze the data for threshold energies. For the present purposes, the data analysis requires that competitive reaction channels be explicitly considered. We accomplish this using a statistical approach that has been described in detail elsewhere[20,21] and is exemplified by eq 1.

$$\sigma_j(E) = (N\sigma_{0,j}/E)\sum g_i \int_{E_{0,j}-E_i}^{E} [k_j(E^*)/k_{\mathrm{tot}}(E^*)] \times P_{D1}(E - \varepsilon)^{N-1}\, \mathrm{d}(\varepsilon) \quad (1)$$

Here, $\sigma_{0,j}$ is an adjustable parameter for channel j that is energy independent, N is an adjustable parameter that describes the energy deposition efficiency during collision,[11] E is the relative kinetic energy of the reactants, $E_{0,j}$ represents the CID threshold energy for channel j at 0 K, and ε is the energy transferred from translation into internal energy of the complex during the collision. E^* is the internal energy of the energized molecule (EM) after the collision, i.e., $E^* = \varepsilon + E_i$, where E_i are the internal energies of the rovibrational states i of the reactant ion with populations g_i and $\sum g_i = 1$. The term, $P_{D1} = 1 - \exp[-k_{\mathrm{tot}}(E^*)\tau]$, is the total dissociation probability of the EM where τ is the experimental time for dissociation, $\sim 5 \times 10^{-4}$ s (as previously measured by time-of-flight studies).[11] Vibrational frequencies and rotational constants of the reactant ions used to calculate E_i and g_i are obtained from the quantum chemical calculations outlined below and in part I (DOI 10.1021/jp911219u). The Beyer−Swinehart−Stein−Rabinovitch algorithm[22] is used to evaluate the density of the rovibrational states, and the relative populations g_i are calculated for a Maxwell−Boltzmann distribution at 300 K. The term $k_j(E^*)$ in eq 1 is the unimolecular rate constant for dissociation of the EM to channel j. The rate constants $k_j(E^*)$ and $k_{\mathrm{tot}}(E^*)$ are defined by Rice−Ramsperger−Kassel−Marcus (RRKM)[23−25] theory in eq 2

$$k_{\mathrm{tot}}(E^*) = \sum k_j(E^*) = \sum d_j N^{\dagger}_{j,vr}(E^* - E_{0,j})/h\rho_{vr}(E^*) \quad (2)$$

where the summation is over all channels j, d_j is the reaction degeneracy for channel j, h is the Planck's constant, $N^{\dagger}_{j,vr}(E^* - E_{0,j})$ is the sum of rovibrational states of the transition state (TS) at an energy $E^* - E_{0,j}$ for channel j, and $\rho_{vr}(E^*)$ is the density of rovibrational states of the EM at the available energy, E^*.

To evaluate the rate constants in eq 2, vibrational frequencies and rotational constants for the EM and all TSs are required. Because the metal−ligand interactions in the complexes studied here are mainly long-range electrostatic interactions (ion−dipole, ion−quadrupole, and ion−induced dipole interactions), the most appropriate model for the TS for channels involving heterolytic cleavage of metal−ligand bonds is a loose association of the ion and neutral ligand,[15,18,26−29] even for multidentate ligands.[30−33] Therefore, the TSs are treated as product-like, with TS frequencies equal to those of the dissociation products, and transitional frequencies treated as rotors in the phase space limit (PSL), as described in part I (DOI 10.1021/jp911219u) and in detail elsewhere.[20,21]

In the Li^+(Cys) system, fragmentation to $Li^+ + Cys$ competes with a lower energy fragmentation process that occurs via a tight TS. For the latter channel, the required molecular parameters are taken from calculations of the reaction pathway, as detailed below. Competition between the two channels is naturally included in eq 1 by the branching ratio term, $k_j(E^*)/k_{\mathrm{tot}}(E^*)$. In addition, this alternate product can dissociate at higher energies to form Li^+. This process depletes the cross section of the low-energy fragmentation reaction and augments that of the Li^+ cross section. This sequential dissociation process can be included in our analysis using a model that has recently been developed.[34] This model makes statistical assumptions regarding the energy deposition in the products of the initial reaction. Ultimately, this model assigns a probability for further dissociation of the initial product, $P_{D2} = 1 - \exp[-k_2(E_2^*)\tau]$, where E_2^* is the internal energy of the product ion undergoing sequential dissociation, EM_2. This energy is determined by energy conservation, i.e., $E_2^* = E^* - E_0 - T_1 - E_L$, where T_1 is the translational energy of the primary products and E_L is the internal energy of the neutral product. Statistical assumptions are used to assign the distributions of each of these quantities, thereby allowing calculation of the secondary dissociation rate constant, k_2. In the present system, the application of the statistical model for sequential dissociation is not rigorously correct, as E_2^* can contain some of the energy released to EM_2 after passing over the tight TS. Therefore, the application of this model may not provide quantitative interpretation of the data but should be sufficient to characterize the qualitative behavior of the sequential dissociation channel.

Before comparing with the experimental data, the cross sections calculated using eq 1 are convoluted over the kinetic energy distribution of the ion beam and thermal energy distribution of the neutral collision gas (Doppler broadening), as described elsewhere.[10] A nonlinear least-squares analysis is used to provide optimized values for $\sigma_{0,j}$, $E_{0,j}$, and N. The uncertainty associated with $E_{0,j}$ is estimated from the range of threshold values determined from different data sets with variations in the parameter N, changes in vibrational frequencies (±10% for most vibrations and a factor of 2 for the M^+−Cys modes), variations in τ by a factor of 2, variations in a frequency scaling factor (see discussion below), and the uncertainty in the absolute energy scale, 0.05 eV (lab).

Computational Details. All calculations were carried out using the Gaussian 03 suite of programs.[35] Structures of the ground state reactant complexes and some intermediates were located using a protocol detailed elsewhere[26] and outlined in part I (DOI 10.1021/jp911219u). The chiral properties of the Cys ligand were constrained throughout our calculations. For the reaction pathway calculations detailed here, transition states were generally determined by relaxed potential energy surface scans (in which a likely reaction coordinate was systematically varied while allowing all other degrees of freedom to freely optimize) at the B3LYP/6-311G(d,p) level.[36,37] Intermediate structures on either side of each TS were confirmed by the character of the potential energy surface scans and examination of the imaginary frequency. Final geometry optimizations and frequency calculations of all reactants, intermediates, and transition states were performed using density functional theory

(DFT) at the B3LYP/6-311G(d,p) level. This level of theory has been shown to be adequate for accurate structural descriptions of comparable metal−ligand systems.[18,26] Single point energy calculations were carried out for all structures at the B3LYP, B3P86, and MP2(full) levels using the 6-311+G(2d,2p) basis set. Zero-point vibrational energy (ZPE) corrections were determined using vibrational frequencies calculated at the B3LYP/6-311G(d,p) level after scaling by 0.9804.[38] Basis set superposition errors (BSSEs) in calculated bond dissociation energies were estimated using the full counterpoise (cp) method.[39,40]

Because the present systems all include lithium, it is important to consider what effects that correlation of the core electrons on lithium might have, as recently elucidated in a comprehensive analysis of lithium cation affinities.[41] Therefore, for selected species, geometries and vibrational frequencies were also calculated at the MP2(full) level of theory with the cc-pCVDZ basis set for Li^+ that include core correlations[42] along with cc-pVDZ[43,44] on all other atoms (designated as cc-pVDZ(C−Li) below), followed by single point calculations using B3LYP, B3P86, and MP2(full) levels with the cc-pCVTZ basis set for Li^+ and aug-cc-pVTZ basis set for other atoms (designated as aug-cc-pVTZ(C−Li) below). No counterpoise corrections are made to the corresponding bond energies, as these have been shown to reduce the accuracy of the MP2 computational results.[41]

3. Results

Cross Sections for Collision-Induced Dissociation. Experimental cross sections for the interaction of Xe with $Li^+(C_3H_7O_2NS)$ as a function of collision energy are shown in Figure 1. At high energies, the dominant dissociation process observed is the loss of the intact amino acid in reaction 3, but there are two other fragmentation products observed at lower energies resulting from reactions 4 and 5.

$$Li^+(C_3H_7O_2NS) + Xe \rightarrow Li^+ + Cys + Xe \quad (3a)$$

$$\rightarrow Li^+(C_3H_4O_2S) + NH_3 + Xe \quad (4)$$

$$\rightarrow Li^+(NH_3) + C_3H_4O_2S + Xe \quad (5)$$

Deamination is a typical decomposition pathway for many protonated amino acids and the lowest energy fragmentation reaction observed for protonated cysteine.[45−48] The energy dependence of these cross sections clearly shows that ammonia loss in reaction 4 is a particularly low-energy process, with the competitive loss of the $C_3H_4O_2S$ fragment in reaction 5 requiring much more energy. The observation of reactions 4 and 5 also suggests that reaction 3b may contribute to the lithium ion product cross section.

$$Li^+(C_3H_7O_2NS) + Xe \rightarrow Li^+ + NH_3 + C_3H_4O_2S + Xe \quad (3b)$$

The magnitudes of the three products observed are highly dependent on the conditions used in the DC/FT source, with the magnitudes of the cross sections for reactions 4 and 5 increasing substantially as the temperature used to vaporize Cys is increased, whereas the cross section for reaction 3 increases

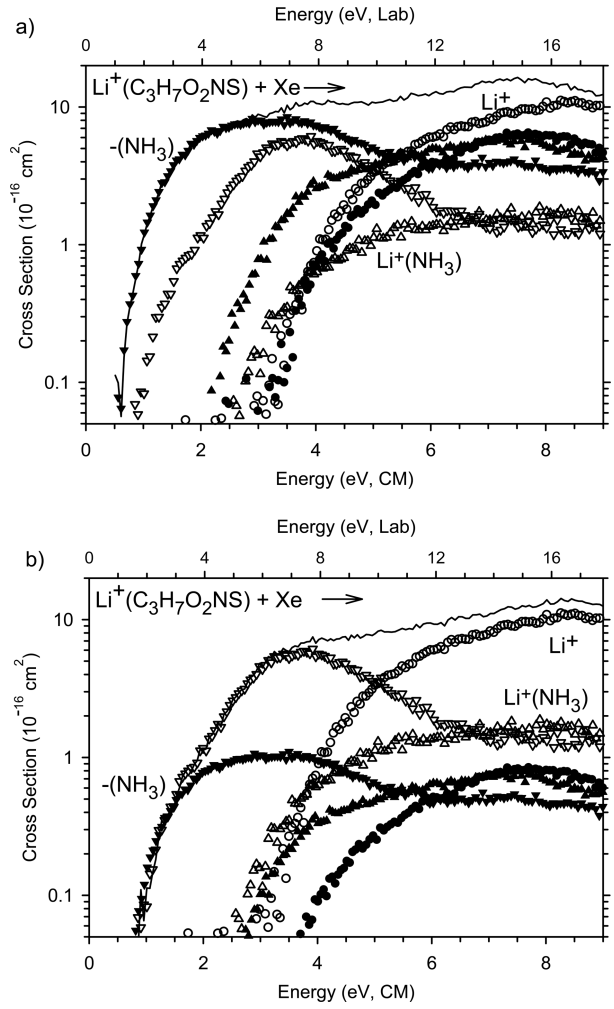

Figure 1. Zero pressure extrapolated cross sections for collision-induced dissociation of $Li^+(C_3H_7O_2NS)$ with xenon as a function of kinetic energy in the center-of-mass frame (lower *x* axis) and the laboratory frame (upper *x*-axis). Symbols show data taken using the flow tube with higher (closed) and lower (open) temperatures used to introduce the cysteine ligand. Part b shows the same cross sections but with the higher temperature data scaled down by a factor of 8. The lines in parts a and b show the total cross sections for the higher and lower temperature data, respectively.

only modestly. It can also be seen that the cross section for reaction 4 associated with reactant ions formed at the lower temperature (open symbols) has two features in the threshold region, with apparent thresholds of about 1 and 2 eV (even more obvious when plotted on a linear scale). The lower energy feature matches the behavior of the higher temperature source conditions (solid symbols), which is demonstrated in Figure 1b, where the higher temperature data for all three channels has been scaled down (multiplied by a factor of 0.13). The presence of these two features suggests that the ions formed in the flow tube source have two distinct populations. We hypothesize that association of Li^+ with Cys heated to induce efficient vaporization allows the deamination to occur in the source, forming a $(NH_3)Li^+(C_3H_4O_2S)$ complex having the same mass as Li^+(Cys). Similar behavior has been noted in several previous alkali metal cation−amino acid systems.[49,50]

To a first approximation, the data taken with a high source temperature appears to be primarily composed of $(NH_3)Li^+$-$(C_3H_4O_2S)$ with smaller contributions of Li^+(Cys), whereas the colder source temperature inverts these relative populations. To obtain a cross section characteristic of the intact amino acid

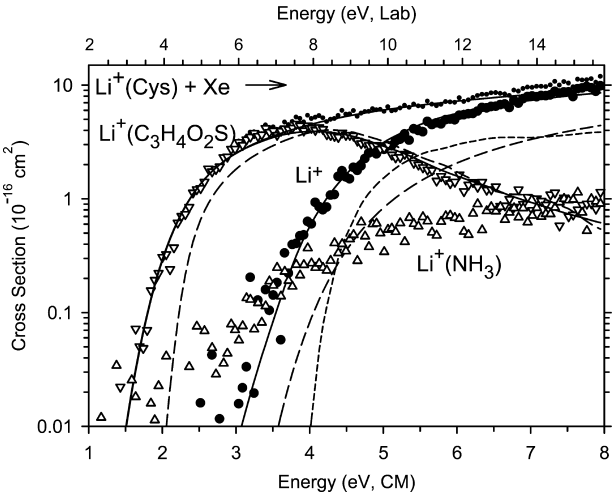

Figure 2. Competitive analysis of the cross sections for collision-induced dissociation of Li^+(Cys); see text. Symbols indicate the experimental cross sections derived by subtracting the scaled higher temperature data from the lower temperature data, with small circles indicating the total cross section above ~3 eV. Solid lines show the model cross sections of eq 1 convoluted over the neutral and ion kinetic and internal energies. Dashed lines show the model cross sections in the absence of experimental energy broadening for reactants with an internal energy of 0 K. The two contributions to the Li^+ cross section are shown by long (reaction 3a) and short (reaction 3b) dashed lines.

complex, we subtract the scaled high-temperature data from the unscaled low-temperature data to obtain the cross sections shown in Figure 2. The hypothesis of two distinct isomers and the resultant deconvolution of the data can be tested by the modeling described below, and eventually by the comparison of the thermochemistry extracted from analysis of the data with theoretical values.

Threshold Analysis and Results. Figure 2 clearly indicates that competition between the loss of the intact amino acid, reaction 3a, and the fragmentation reactions 4 and 5 is possible in the Li^+(Cys) system. Despite the lower energies of reactions 4 and 5, reaction 3 is the dominant reaction at high energies, indicating that this process is entropically favored, consistent with reaction 3a. This is also indicated by the observation that the energy dependence of the $Li^+(C_3H_4O_2S)$ cross section is influenced once reaction 3 becomes accessible. We modeled the data using eq 1 but ignored reaction 5 because the magnitude of its cross section is too small for it to appreciably affect reaction 3 or 4. Despite this simplification, analysis of these cross sections is complicated by the fact that both reactions 3a and 3b can contribute to the Li^+ cross section in an unknown distribution. Therefore, the data were modeled in several ways, Table 1. First, we explicitly included the competition between reactions 3a and 4 but neglected 3b. This approach reproduces the data reasonably well until about 5 eV, at which point the experimental Li^+ cross section begins to exceed the model, suggesting a contribution from reaction 3b. Second, the data were modeled considering only reactions 3b and 4. Again, the data can be reproduced reasonably well until about 5 eV, but now the decline in the $Li^+(C_3H_4O_2S)$ cross section is too slow, suggesting that reaction 3a is needed to also compete with this reaction.

Third, the data was modeled including the competition between reactions 3a and 4 along with the subsequent dissociation of the $Li^+(C_3H_4O_2S)$ product in reaction 3b. An example of this competitive modeling for Li^+(Cys) is shown in Figure 2. Now, the data for the two channels are reproduced very well from about 1 to over 7 eV using the parameters listed in Table 1. In all of these models, both reactions 3a and 3b were assumed to be controlled by loose PSL transition states, with molecular parameters taken directly from quantum calculations. For reaction 4, a detailed theoretical exploration of the pathway for the deamination reaction is conducted below. The molecular parameters of the tight transition state needed here to characterize ammonia loss were taken from these calculations, although the vibrational frequencies needed to be tightened from those calculated in order to accurately reproduce the data (an alternative to using individual scaling factors, $\sigma_{0,j}$ in eq 1, as discussed elsewhere[51]). Specifically, frequencies below 625 cm^{-1} were scaled by a factor of 1.6 ± 0.3 in the two models where reaction 3a was included and 1.3 ± 0.2 when only reaction 3b was included. (This arbitrary frequency limit is chosen in part because the output of the Gaussian program[35] warns that thermodynamic functions may be in error for vibrational frequencies under 625 $cm^{-1} \equiv 900$ K, in large measure because such vibrations may no longer be treated accurately as harmonic at temperatures of interest. In the present system, at the lowest kinetic energy where deamination products are first seen in the absence of energy broadening, about 2 eV, Figure 2, the average energy available to the tight TS corresponds to a temperature of about 5200 ± 800 K.) The need for scaling frequencies <625 cm^{-1} indicates that the calculated harmonic frequencies for the deamination TS provide a somewhat too "loose" characterization of this channel relative to the PSL TSs for reactions 3a and 3b.

As described in more detail below, we have also explored alternative reaction pathways for ammonia loss involving distinct transition states. These TSs are calculated to be >0.6 eV higher in energy than the lowest transition state, but when molecular parameters for these alternative TSs are used in eqs 1 and 2, the E_0 thresholds obtained do not change appreciably, with differences <0.08 eV. Such results indicate that the measured threshold energies are insensitive to the choice of tight TS or the detailed molecular parameters used.

Table 1 also includes parameters of eq 1 when the Li^+ cross section is modeled ignoring competition with reaction 4. Comparison of the thresholds with and without competition included shows that the competition lowers the threshold for Li^+ production by ~0.5 eV, which correctly reflects the expected effect of competition on the higher energy Li^+ channel. (If the kinetics of dissociation are also excluded, the threshold increases by another 0.8 eV.) This competitive shift is slightly larger than observed previously for the Li^+(Ser), Li^+(Thr), and Li^+(Met) systems where it was ~0.3 eV.[52,53] In addition, the N value is close to unity for two of the competitive analyses (reactions 3b + 4 and 3a + 3b + 4), smaller than the single channel modeling results ($N = 1.4$). As demonstrated previously, the parameter N characterizes the energy deposition efficiency upon collision,[11] with a smaller number indicating better energy transfer efficiency and a value near unity corresponding to the line-of-centers model. The value of $N = 0.6$ used for the competitive analysis with reactions 3a + 4 is unusually low for a system having a threshold above 1 eV and is needed primarily to match the decline in the $Li^+(C_3H_4O_2S)$ cross section at higher energies. The small N parameter generally gives higher thresholds, which is consistent with the observation that this model does not reproduce the threshold cross section for reaction 4 as well as the other two competitive models. We note that the threshold energy for reaction 4 is relatively insensitive to the various model assumptions, varying by only ~0.1 eV. The thresholds for reactions 3a and 3b vary more appreciably because the interpretation depends critically on the assumptions used. The

TABLE 1: Fitting Parameters of eq 1, Threshold Dissociation Energies at 0 K, and Entropies of Activation at 1000 K for CID of $M^+(C_3H_7O_2NS)$ with Xe[a]

reactant	products	σ_0	N	E_0 (eV)	$\Delta S^{\ddagger}_{1000}$ (J/mol K)
Li^+(Cys)	$Li^+ + Cys$	10.5 (1.3)	1.4 (0.1)	3.16 (0.17)[b]	50 (2)
Li^+(Cys)[c]	$Li^+(C_3H_4O_2S) + NH_3$	15.0 (2.0)	0.6 (0.1)	1.78 (0.15)	−20 (20)
	$Li^+ + Cys$	15.0 (2.0)	0.6 (0.1)	3.01 (0.14)	50 (2)
Li^+(Cys)[d]	$Li^+(C_3H_4O_2S) + NH_3$	10.4 (2.4)	1.0 (0.2)	1.83 (0.15)	5 (20)
	$Li^+ + C_3H_4O_2S + NH_3$	16.1 (2.1)	1.0 (0.2)	3.54 (0.25)	
Li^+(Cys)[e]	$Li^+(C_3H_4O_2S) + NH_3$	9.7 (2.9)	1.1 (0.2)	1.72 (0.18)	−20 (20)
	$Li^+ + Cys$	9.7 (2.9)	1.1 (0.2)	2.65 (0.12)	50 (2)
	$Li^+ + C_3H_4O_2S + NH_3$	88 (68)	1.1 (0.2)	3.84 (0.28)	
$(NH_3)Li^+(C_3H_4O_2S)$	$Li^+(C_3H_4O_2S) + NH_3$	10.4 (0.6)	1.2 (0.1)	1.13 (0.04)	5 (5)
	$Li^+(NH_3) + C_3H_4O_2S$	506 (152)	1.2 (0.1)	1.75 (0.06)	28 (5)
	$Li^+ + C_3H_4O_2S + NH_3$	49.3 (6.8)	1.2 (0.1)	3.47 (0.08)	

[a] Uncertainties are listed in parentheses. [b] If lifetime effects are not included, a threshold of 3.96 ± 0.22 eV is obtained. [c] Competitive fitting results for cross sections of reactions 3a and 4; see text for details. [d] Competitive fitting results for cross sections of reactions 3b and 4; see text for details. [e] Competitive fitting results for cross sections of reactions 3a, 3b, and 4; see text for details.

different models tried here make it clear that reaction 3a has a lower threshold than reaction 3b (a result consistent with theory), which indicates that the onset observed for the Li^+ cross section in Figure 2 should correspond to reaction 3a and therefore reaction 3a cannot be ignored (as in the 3b + 4 competitive model). Conservatively, the thresholds obtained using single channel fitting and the reaction 3a + 4 competitive model should be viewed as upper limits to the thermodynamic threshold for reaction 3a. We believe that the reaction 3a + 3b + 4 competitive modeling results provide the best values from the present experiments. As discussed below, this competitive modeling value for reaction 3a is in good agreement with theoretical values, and as discussed in part I (DOI 10.1021/jp911219u),[1] this value agrees with various trends in the bond energies for different metal cations and amino acids. For reaction 3b, the threshold obtained from this model may be flawed because the statistical sequential dissociation model is not rigorously correct for subsequent dissociation after a tight TS, as noted above.

The data taken at high flow tube temperatures, i.e., the data purported to correspond primarily to the $(NH_3)Li^+(C_3H_4O_2S)$ complex, can also be modeled. The processes considered include the competition between loss of ammonia from the $(NH_3)Li^+(C_3H_4O_2S)$ complex (reaction 4) and loss of the $C_3H_4O_2S$ fragment from the $(NH_3)Li^+(C_3H_4O_2S)$ complex (reaction 5), along with the subsequent dissociation of both products to $Li^+ + C_3H_4O_2S + NH_3$ (reaction 3b). (Here, application of the statistical model for sequential dissociation is appropriate, as the primary dissociation occurs over a loose PSL TS.) The results of this modeling are illustrated in Figure 3 with the optimized parameters listed in Table 1. It can be seen that all three data channels are accurately reproduced over extensive energy and magnitude ranges. Details of the modeling shown include the assumption that the $C_3H_4O_2S$ fragment and its associated complexes has the thiirane structure, as detailed in the theory section below. Also, the CRUNCH program used to analyze the data is limited to a single sequential dissociation channel. Therefore, the formation of Li^+ in reaction 3b is modeled exclusively as coming from the initial $Li^+(C_3H_4O_2S)$ product ion, because the intensity of this product far exceeds that for $Li^+(NH_3)$.

Also shown in Table 1 are the entropies of activation at 1000 K for these analyses. The values obtained properly reflect the differences between the loose PSL TSs, which generally have $\Delta S^{\ddagger}$ values of 28−50 J/(mol K), and the tight TS, where the $\Delta S^{\ddagger}$ value is −20 J/(mol·K). The $\Delta S^{\ddagger}$ value for loss of NH_3 from the $(NH_3)Li^+(C_3H_4O_2S)$ complex is lower than that found

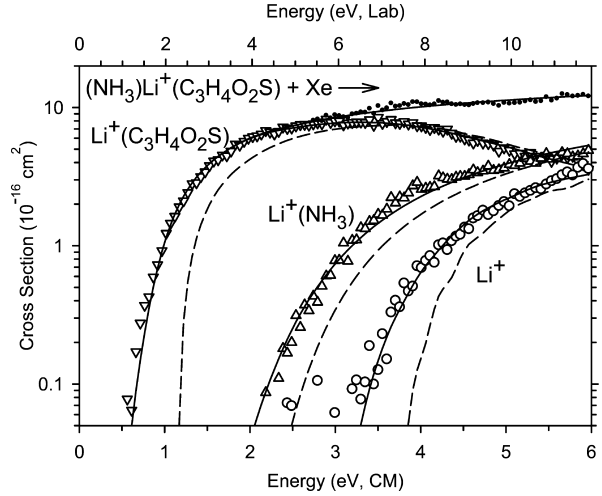

Figure 3. Competitive analysis of the cross sections for collision-induced dissociation of $(NH_3)Li^+(C_3H_4O_2S)$; see text. Symbols indicate the experimental cross sections taken at the higher temperature for cysteine introduction, with small circles indicating the total cross section above ~2.5 eV. Solid lines show the model cross sections of eq 1 convoluted over the neutral and ion kinetic and internal energies. Dashed lines show the model cross sections in the absence of experimental energy broadening for reactants with an internal energy of 0 K.

for the other loose TSs examined here but is comparable to those obtained for loss of a water ligand from $(H_2O)_nNa^+$(Gly) and $(H_2O)_nNa^+$(Pro),[29,54] as well as for loss of water or ammonia from analogous complexes formed in the dissociation of lithiated Ser and Thr[49] and sodiated Asp, Asn, Glu, and Gln.[50] This entropy is therefore consistent with the suggested bis-ligated structure.

Theory: $C_3H_4O_2S$, $Li^+(C_3H_4O_2S)$, and $(NH_3)Li^+(C_3H_4O_2S)$. To discuss the deamination reaction observed experimentally, we need to consider various possible structures of the $C_3H_4O_2S$ and its complexes. Quantum chemical calculations on all of these species were performed as described above, using the same level of theory as those for Li^+(Cys) in part I (DOI 10.1021/jp911219u).

Several possible isomers for $C_3H_4O_2S$ formed by deamination of Cys were considered and include 3-mercaptopropenoic acid (Mpa), thioacetaldehyde-2-carboxylic acid (Taca), the three-membered ring thiirane-carboxylic acid (Tica), and 3-mercapto-α-propiolactone (Mpl), Figure 4 and Table 2. Some of these possibilities were guided by the previous work by O'Hair and co-workers and Ohanessian and co-workers on the deamination reactions of protonated cysteine.[48,55] The $C_3H_4O_2S$ species with

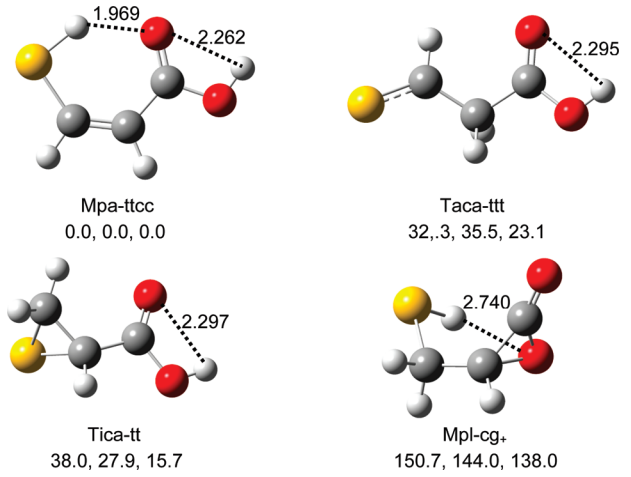

Figure 4. Optimized structures of $C_3H_4O_2S$ calculated at the B3LYP/6-311G(d,p) level of theory. Relative energies in kJ/mol calculated at the B3LYP, B3P86, and MP2(full) levels of theory with zero point energy corrections included are shown. Dashed lines show hydrogen bonds with bond lengths indicated in Å.

TABLE 2: Relative Energies (kJ/mol) of Low-Lying Conformers of the $C_3H_4O_2S$ Fragment Obtained from Cys

		theory[a]		
fragment[b]	structure	B3LYP	B3P86	MP2(full)
$HSC_2H_2CO_2H$ (Mpa)	ttcc	0.0	0.0	0.0
	tttc	5.6	8.1	7.4
	tctc	7.3	10.0	8.6
	tccc	13.6	15.3	13.4
	tcct	15.7	17.9	15.3
	ctcc	20.5	20.1	20.8
$HCSCH_2$-2-CO_2H (Taca)	ttt	32.3	35.5	23.1
	tcg	34.8	38.3	24.3
	tgc	39.8	43.1	26.3
	ccc	43.8	43.2	35.9
c-SC_2H_3-CO_2H (Tica)	tt	38.0	27.9	15.7
	tc	40.1	29.8	17.2
	cg	45.2	32.2	21.1
c-$OCOCHCH_2SH$ (Mpl)	cg_+	150.7	144.0	138.0
	cg_-	150.7	144.0	142.1
	tt	149.5	144.1	143.3

[a] Structures are optimized at the B3LYP/6-311G(d,p) level and zero point energies calculated at this level are included in all values. Single point energies are calculated using the indicated level of theory and the 6-311+G(2d,2p) basis set. [b] Selected structures shown in Figure 4.

the lowest energy is Mpa, which has five isomers having a OH···OC hydrogen bond. These isomers are designated by the HOCC, OCCC, CCCS, and CCSH dihedral angles (c = cis for <50°, g = gauche for angles between 50 and 135°, and t = trans for >135°) as ttcc, tttc, tctc, tccc, and tcct. At all three levels of theory, the ground state (GS) structure has a ttcc geometry allowing a SH···OC hydrogen bond, Figure 4, whereas the four other conformers lie higher in energy by 5−18 kJ/mol, Table 2. In addition, there are comparable structures in which the hydroxyl group has rotated such that there is no OH···OC hydrogen bond. The lowest of these, Mpa-ctcc, was located 20−21 kJ/mol above Mpa-ttcc, Table 2, and a comparable difference is anticipated between other variants.

The next lowest energy fragment is Taca, for which four isomers were located: ttt, tcg, tgc, and ccc (as designated using the HOCC, OCCC, and CCCS dihedral angles). These lie 23−36 kJ/mol above the Mpa-ttcc GS at the MP2 level of theory and 32−44 kJ/mol higher at the DFT levels. In three of these (ttt, tcg, and ccc), the heavy atoms lie more or less in a plane, where the first two structures have a OH···OC hydrogen bond and the latter a OH···S hydrogen bond. In the tgc isomer, which retains a OH···OC hydrogen bond, the plane of the carboxylic acid is nearly perpendicular to the CCCS plane. Isomers having ttc and tcc arrangements were also investigated and collapse to tgc and ccc, respectively.

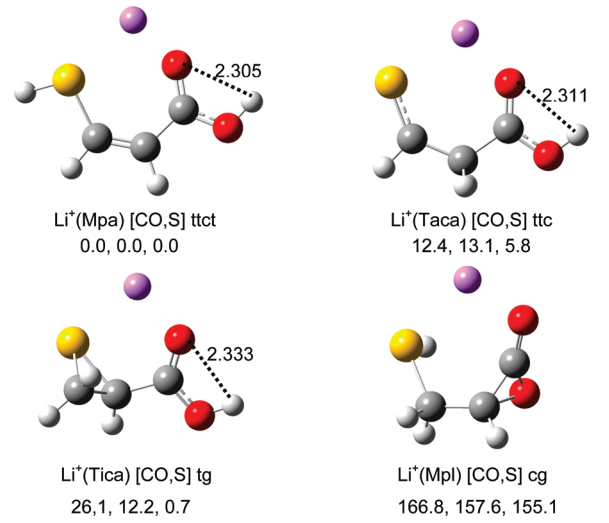

Figure 5. Optimized structures of $Li^+(C_3H_4O_2S)$ calculated at the B3LYP/6-311G(d,p) level of theory. Relative energies in kJ/mol calculated at the B3LYP, B3P86, and MP2(full) levels of theory with zero point energy corrections included are shown. Dashed lines show hydrogen bonds with bond lengths indicated in Å.

Similar in energy to Taca (and lower at the B3P86 and MP2 levels) is Tica, for which three isomers were located: tt, tc, and cg (as designated by HOCC and OCCC dihedral angles). These lie 15−21 kJ/mol above the Mpa-ttcc GS at the MP2 level of theory, 28−32 kJ/mol at B3P86, and 38−45 at B3LYP. The two low-lying conformers both have OH···OC hydrogen bonds, whereas the higher lying cg conformer has a OH···S hydrogen bond. Finally, the lactone (Mpl) conformers all have similar energies, within 5 kJ/mol at a particular level of theory, and lie 138−151 kJ/mol above Mpa. The cg_+ and cg_- conformers (as designated by CCCS and CCSH dihedral angles, with ± indicating the sign of the angle) have the sulfur group cis with the lactone ring, whereas they are trans in the tt conformer.

When Li^+ binds to these fragments, there are again a multitude of conformers as listed in Table 3. These are designated by the metal cation binding sites in square brackets along with the same dihedral angle designations used above. Figure 5 shows the lowest energy structures for each type of ligand, with relative energies and metal−ligand bond distances of all species in Table 3. For Mpa, we located five conformers. The two having the lowest and highest energy, [CO,S] ttct and [CO,S] ctct, bind the lithium cation to both the carbonyl and sulfur, whereas the middle three conformers only bind at the carbonyl site. The three lowest energy structures all have OH···OC hydrogen bonds, whereas the ccct structure has a OH···S hydrogen bond. In the high-energy ctct structure, the hydroxyl group has been rotated ~180° from the ttct geometry, such that there is no hydrogen bonding.

Three conformers of Li^+(Taca) were located with [CO,S] ttc being 18−24 kJ/mol lower in energy than [CO] ccc. The former has a OH···OC hydrogen bond, whereas the latter has a OH···S hydrogen bond. The [CO,S] ctc structure, which has neither hydrogen bond, lies 20−21 kJ/mol above the ttc conformer. When either the tcg or tgc conformers of Taca were bonded to

TABLE 3: Geometric Parameters and Relative Energies (kJ/mol) of Low-Lying Conformers of the $Li^+(C_3H_4O_2S)$ Product Obtained from Li^+(Cys)

				theory[a]		
complex[b]	structure	$r(Li^+-O)$ (Å)	$r(Li^+-S)$ (Å)	B3LYP	B3P86	MP2(full)
Li^+(Mpa)	[CO,S] ttct	1.786	2.481	0.0	0.0	0.0
	[CO] tctc	1.722		6.2	6.1	13.6
	[CO] tttc	1.722		11.3	12.5	19.6
	[CO] ccct	1.743		20.3	18.9	22.0
	[CO,S] ctct	1.745	2.680	35.9	33.9	35.9
Li^+(Taca)	[CO,S] ttc	1.812	2.404	12.4	13.1	5.8
	[CO,S] ctc	1.797	2.429	33.7	34.3	26.2
	[CO] ccc	1.759		36.4	31.8	26.3
Li^+(Tica)	[CO,S] tg	1.849	2.497	26.1	12.2	0.7
	[CO] cg	1.757		49.1	33.2	24.3
	[OH,S] tg	1.900	2.403	71.6	60.2	40.3
	[CO_2^-] cc	1.939	1.977[c]	95.6	81.9	71.8
Li^+(Mpl)	[CO,S] cg	1.854	2.635	166.8	157.6	155.1
	[O,S] ct	1.902	2.492	192.0	184.1	175.6

[a] Structures are optimized at the B3LYP/6-311G(d,p) level, and zero point energies calculated at this level are included in all values. Single point energies are calculated using the indicated level of theory and the 6-311+G(2d,2p) basis set. To obtain energies for these complexes + NH_3 relative to Li^+(Cys) [N,CO,S], add 67.1, 89.1, and 106.7 kJ/mol for B3LYP, B3P86, and MP2(full) values, respectively. [b] Selected structures shown in Figure 5. [c] $Li^+-O\cdots HS$.

TABLE 4: Geometric Parameters and Relative Energies (kJ/mol) of Low-Lying Conformers of $(NH_3)Li^+(C_3H_4O_2S)$ Complexes

					theory[a]		
species	structure	$r(Li^+-O)$ (Å)	$r(Li^+-S)$ (Å)	$r(Li^+-N)$ (Å)	B3LYP	B3P86	MP2(full)
$(NH_3)Li^+$(Mpa)	[CO] tctc	1.765		2.011	0.0 (−49.9)	0.0 (−24.0)	6.8 (−5.9)
	[CO,S] ttct	1.807	2.673	2.014	3.0 (−46.9)	0.2 (−23.8)	0.0 (−12.7)
	[CO] tttc	1.763		2.012	5.0 (−44.9)	5.1 (−18.9)	11.9 (−0.8)
	[CO] tttt	1.765		2.011	7.1 (−42.8)	7.3 (−16.7)	14.7 (2.0)
	[CO] ccct	1.791		2.009	16.0 (−33.9)	13.6 (−10.4)	16.5 (3.8)
$(NH_3)Li^+$(Taca)	[CO,S] ttc	1.859	2.465	2.019	20.5 (−29.4)	19.4 (−4.6)	8.7 (−4.0)
$(NH_3)Li^+$(Tica)	[CO,S] tg	1.893	2.575	2.014	29.4 (−20.5)	14.1 (−9.9)	0.3 (−12.4)
	[CO] cg	1.803		2.006	41.3 (−8.6)	24.3 (0.3)	16.2 (3.5)
	[CO,S] cg	1.872	2.625	2.012	48.6 (−1.3)	33.2 (9.2)	20.1 (7.4)
	[CO] tc	1.789		2.006	53.1 (3.2)	40.0 (16.0)	31.0 (18.3)
	[CO_2^-] cc	1.983	2.044[b]	2.016	103.7 (53.8)	87.4 (63.4)	78.5 (65.8)

[a] Structures are optimized at the B3LYP/6-311G(d,p) level, and zero point energies calculated at this level are included in all values. Single point energies are calculated using the indicated level of theory and the 6-311+G(2d,2p) basis set. Energies relative to Li^+(Cys) [N,CO,S] are given in parentheses. [b] $Li^+-O\cdots HS$.

Li^+, they collapsed to the ttc structure. Li^+(Taca) [CO,S] ttc lies only 6−13 kJ/mol above Li^+(Mpa) [CO,S] ttct. Four conformers of Li^+(Tica) were found with the lowest, [CO,S] tg, lying 0.7−26 kJ/mol above Li^+(Mpa) [CO,S] ttct. In [CO,S] tg and [OH,S] tg, the lithium cation binds bidentate to the sulfur and either the carbonyl or hydroxyl group of the carboxylic acid, with a $OH\cdots OC$ hydrogen bond in both. The hydroxyl group binds much more weakly than the carbonyl such that [OH,S] tg lies 40−48 kJ/mol above [CO,S] tg. In the [CO] cg structure, lithium binds only to the carbonyl and there is a $OH\cdots S$ hydrogen bond. As this proton moves to the sulfur to form a zwitterionic ligand, the lithium bends around to interact with both carboxylate oxygens in the [CO_2^-] cc structure. These two species lie 21−24 kJ/mol and ∼70 kJ/mol, respectively, above Li^+(Tica) [CO,S] tg. Finally, as for the neutral fragments, the Mpl lactone complexes lie high in energy, 155−192 kJ/mol above Li^+(Mpa) [CO,S] ttct. Both structures located are bidentate, with the [CO,S] cg structure being 20−27 kJ/mol lower in energy than [O,S] ct, where lithium binds to the lactone ring oxygen.

The ground states of all $(NH_3)Li^+(C_3H_4O_2S)$ systems considered here have the ammonia molecule binding directly to the other side of Li^+ while keeping the rest of the molecule nearly unchanged from the structures shown in Figure 5. The relative energies of the species located are listed in Table 4, along with metal ligand bond distances. Not all possible isomers of $C_3H_4O_2S$ were considered, but the lowest energy conformations of $(NH_3)Li^+$(Mpa), $(NH_3)Li^+$(Taca), and $(NH_3)Li^+$(Tica) were included explicitly. Even though all possible conformations were not calculated directly, as will be seen below, the binding energy of ammonia to $Li^+(C_3H_4O_2S)$ is insensitive to the identity of the $C_3H_4O_2S$ ligand, such that the energy ordering of $(NH_3)Li^+(C_3H_4O_2S)$ complexes should parallel that of $Li^+(C_3H_4O_2S)$ complexes, discussed above. Among the systems explored, the $(NH_3)Li^+$(Mpa) system is the lowest in energy, with the [CO] tctc and [CO,S] ttct conformers being similar in energy. The former lies lower than the ground state of Li^+(Cys) by 6−50 kJ/mol and is the DFT ground state, whereas the bidentate [CO,S] conformer is 13−47 kJ/mol lower than Li^+(Cys) and is the ground state at the MP2(full) level of theory, Table 4. Alternate conformations, [CO] tttc, [CO] tttt, and [CO] ccct, lie 5−12, 4−15, and 13−17 kJ/mol, respectively, higher than the GSs. The lowest energy $(NH_3)Li^+$(Taca) conformer lies 4−30 kJ/mol below Li^+(Cys) and 9−20 kJ/mol above the $(NH_3)Li^+$(Mpa) GS. Several conformations of $(NH_3)Li^+$(Tica) were examined, as these lie along the minimum energy pathway located for dissociation of Li^+(Cys); see below. The lowest of these, [CO,S] tg, lies 10−21 kJ/mol below Li^+(Cys) and 0−29 kJ/mol above the $(NH_3)Li^+$(Mpa) GS. The variant in which the $OH\cdots OC$ hydrogen bond has been broken by rotation of the

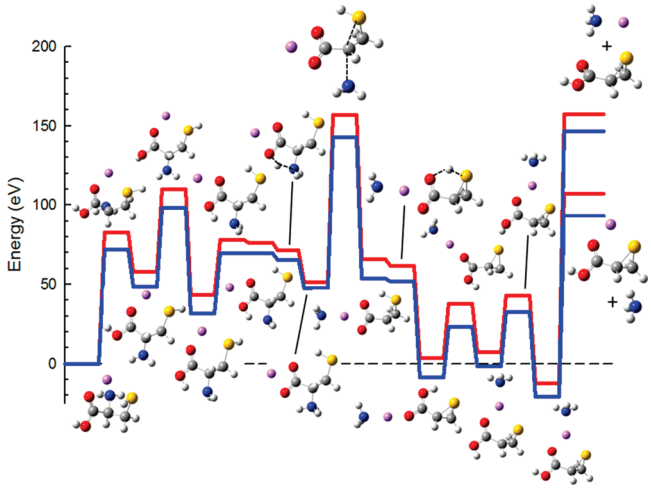

Figure 6. Calculated potential energy surface for the lowest energy pathway for loss of NH_3 from Li^+(Cys) at the B3LYP (blue) and MP2(full) (red)/6-311+G(2d,2p)//B3LYP/6-311G(d,p) levels of theory including zero point energy corrections. The structures of all intermediates are shown below the surface, and those for transition states are shown above.

hydroxyl group, [CO,S] cg, lies 19−20 kJ/mol higher, whereas two monodentate structures, [CO] cg and [CO] tc, lie higher by 10−16 and 24−31 kJ/mol, respectively. The former has a OH···S hydrogen bond, whereas the latter retains a OH···OC hydrogen bond. Finally, a zwitterionic [CO_2^-] cc conformation was found 73−78 kJ/mol above (NH_3)Li^+(Tica) [CO,S] tg.

Deamination of Li^+(Cys). In order to elucidate the reaction mechanism for deamination of Cys in reactions 4 and 5 and to provide molecular parameters for the TS associated with this process (used for modeling of reaction 4), a series of reaction path calculations were performed.

The lowest energy reaction pathway found for deamination is the transfer of a hydrogen atom from the carboxylic acid to the amino group followed by NH_3 elimination assisted by backside attack at C_α by the sulfur side chain (a so-called 3-exotet cyclization).[56,57] This pathway has similarities to that located for deamination of protonated cysteine with the lithium cation replacing the proton on the carboxylic acid.[48,55] The complete reaction coordinate diagram including all TSs and intermediates along this pathway is presented in Figure 6. Relative energies calculated for all intermediates (INTs) and transition states (TSs) calculated at three levels of theory can be found in Table 5 along with some critical geometric parameters and imaginary frequencies for all TSs. Starting with the tridentate Li^+(Cys) [CO,N,S] $tggg_+$ ground state (GS) complex,[1] the first step rotates the OCCN dihedral angle in order to move the amino ligand away from the lithium cation. TS[∠OCCN] lies 72−83 kJ/mol above the GS and forms the bidentate Li^+(Cys) [CO,S] ttgt conformer at a relative energy of 49−58 kJ/mol. To allow proton transfer to the amino group, the hydroxyl group is now rotated 180° to form Li^+(Cys) [CO,S] ctgt, which lies 30−44 kJ/mol above the GS. This replaces a OH···OC hydrogen bond with a OH···N hydrogen bond. Next, the lithium cation moves from the [CO,S] binding site to the [COOH] binding site, which also permits the thio group to rotate such that a SH···OC hydrogen bond is formed in the next intermediate, [COOH] ctg_+g_-. This motion costs 34−38 kJ/mol, where the TS[∠LiOC] involved is only 0−2 above the intermediate formed. Furthermore, the proximity of the lithium cation to the hydroxyl group in [COOH] ctg_+g_- facilitates transfer of the proton from the hydroxyl to the amino group. Indeed, once zero point energies are included, the TS for this proton motion lies 4−7 kJ/mol lower in energy and readily forms the zwitterionic [CO_2^-] ctg_+g_- intermediate lying 19−25 kJ/mol lower than the [COOH] ctg_+g_- charge-solvated analogue (47−52 kJ/mol above the GS).

From the zwitterionic [CO_2^-] ctg_+g_- intermediate, ammonia loss readily occurs by cleavage of the C_α−NH_3 bond (changing from 1.531 Å in the intermediate to 2.537 Å at the TS), a process that is assisted by backside attack of the sulfur at the α carbon (such that the C_α−S bond length changes from 2.810 to 2.074 Å at the TS and 1.886 Å for the thiirane complex formed). This is the rate-limiting TS along the pathway shown in Figure 6 and lies 143−157 kJ/mol above the GS. This process forms the thiirane-carboxylic acid (Tica) isomer of $C_3H_4O_2S$, initially in the zwitterionic form with a SH···O hydrogen bond. As the ammonia group migrates to a stable position on the lithium cation opposite the $C_3H_4O_2S$ ligand, the (NH_3)Li^+(Tica) [CO_2^-] cc conformer is formed. However, once zero point energies are included, the TS for moving the proton from sulfur to the carboxylic acid lies 2−5 kJ/mol lower in energy, such that the charge solvated (NH_3)Li^+(Tica) [CO] cg complex is readily formed. This species is more stable than the zwitterionic form by 62−69 kJ/mol and lies between −9 and +4 kJ/mol compared to the Li^+(Cys) GS reactant. Rotation about the CC bond, which requires 32−36 kJ/mol, now brings the lithium cation into proximity of the sulfur atom, allowing formation of (NH_3)Li^+(Tica) [CO,S] cg. Rotation of the hydroxyl group, which requires 34−36 kJ/mol, then forms the lowest energy conformer of (NH_3)Li^+(Tica), [CO,S] tg, lying 10−21 kJ/mol below the GS reactants. Note that this species is the global minimum on this potential energy surface. We also explored whether the rotation of the hydroxyl group might occur first from the (NH_3)Li^+(Tica) [CO] cg intermediate to form a (NH_3)Li^+(Tica) [CO] tg complex, but this requires more energy than the pathway shown, with a TS at 48−65 kJ/mol above the GS reactants.

From (NH_3)Li^+(Tica) [CO,S] tg, the ammonia ligand can be lost readily to form Li^+(Tica) [CO,S] tg + NH_3. At higher energies, the Tica ligand can be lost from any of the last several intermediates; however, formation of the lowest energy conformer, Tica tt, should occur with the least rearrangement from (NH_3)Li^+(Tica) [CO,S] tg. Note that the energy of the Li^+(Tica) [CO,S] tg + NH_3 asymptote lies well below the energy of the rate-limiting TS, whereas formation of $Li^+(NH_3)$ + Tica is nearly isoenergetic, lying only 0.2−3.7 kJ/mol above the energy of TS[NH_3 loss]. This near degeneracy is qualitatively in agreement with the data in Figure 2, which shows that the apparent threshold for $Li^+(NH_3)$ formation does extend down to energies approaching the onset for $Li^+(C_3H_4O_2S)$ + NH_3 formation, which is limited by TS[NH_3 loss]. Production of the latter product is much more efficient because it has a much higher number of states available compared to the higher energy reaction forming $Li^+(NH_3)$ + $C_3H_4O_2S$.

Alternate Pathways for Deamination of Li^+(Cys). Several alternative pathways were also explored for reactions 4 and 5, and the transition states located and discussed below are shown in Figure S1 of the Supporting Information. In particular, given the relative stability of the mercaptopropenoic acid (Mpa) product, we considered several pathways to this species. The most likely of these starts with either the zwitterionic [CO_2^-] ctg_-g_- or cgtg form of Li^+(Cys). These species are similar to the [CO_2^-] ctg_+g_- intermediate shown in Figure 6 but rotated around the C_α−C_β bond such that a hydrogen atom on C_β is in a position to transfer to the carboxylate. As proton transfer occurs, a concerted loss of the NH_3 group leads directly to the

TABLE 5: Geometric Parameters and Relative Energies (kJ/mol) for Intermediates, Transition States, and Products for NH_3 Loss from Li^+(Cys)[a]

species[b]	$r(Li^+-O)$ (Å)	$r(Li^+-X)$[c] (Å)	$r(Li^+-N)$ (Å)	B3LYP	B3P86	MP2(full)
Li^+(Cys) [N,CO,S] $tggg_+$	1.938	2.557 S	2.068	0.0	0.0	0.0
TS [∠OCCN] (122i)	1.821	2.425 S		71.9	74.2	82.6
Li^+(Cys) [CO,S] ttgt	1.819	2.407 S		48.8	49.7	58.2
TS [∠HOCO] (673i)	1.823	2.423 S		98.4	101.1	109.8
Li^+(Cys) [CO,S] ctgt	1.786	2.456 S		31.9	30.4	43.7
TS [∠LiOC] (102i)	1.854	2.434 O		69.7	66.3	78.3
Li^+(Cys) [COOH] ctg_+g_-	1.917	2.096 O		69.5	66.3	76.3
TS [CS-ZW] (805i)	1.927	2.042 O		65.5	59.1	71.7
Li^+(Cys) [CO_2^-] ctg_+g_-	1.931	1.960 O		47.5	46.8	51.6
TS [NH_3 loss] (175i)	1.940	1.932 O		**143.0**	**151.7**	**156.9**
$(NH_3)Li^+$(Tica) [CO_2^-] cc	1.983	2.044 O	2.016	53.8	63.4	65.8
TS [ZW-CS] (265i)	1.978	2.065 O	2.016	51.9	58.4	61.8
$(NH_3)Li^+$(Tica) [CO] cg	1.803		2.006	−8.6	0.3	3.5
TS [∠OCCC] (52i)	1.791		2.005	23.3	35.7	37.9
$(NH_3)Li^+$(Tica) [CO,S] cg	1.872	2.625 S	2.012	−1.3	9.2	7.4
TS [∠HOCO] (673i)	1.902	2.581 S	2.011	32.9	44.3	43.2
$(NH_3)Li^+$(Tica) [CO,S] tg	1.893	2.575 S	2.014	−20.5	−9.9	−12.4
Li^+(Tica) [CO,S] tg + NH_3	1.849	2.497 S		93.2	101.3	107.4
$Li^+(NH_3)$ + Tica tt			1.968	146.7	153.3	157.1

[a] Species follow the reaction coordinate of Figure 6. Values determined using geometries and zero point energies calculated at B3LYP/6-311G(d,p) with single point energies calculated at the level shown using the 6-311+G(2d,2p) basis set. [b] For TSs, the imaginary frequency is given in cm^{-1}. [c] X = S or O, as shown.

π-bond between C_α and C_β found in mercaptopropenoic acid. Starting with [CO_2^-] ctg_-g_- leads to the cis-substituted Mpa (ttct), whereas [CO_2^-] cgtg leads to the trans-substituted Mpa (tctc). Both transition states were located and found to be of comparable energy, 250−265 and 253−273 kJ/mol above GS reactants (96−108 and 99−116 kJ/mol above TS[NH_3 loss]), respectively. We believe the high energy of these transition states can partially be attributed to the fact that the carboxylate needs to lie in a plane perpendicular to the incipient π-bond in order to accept the proton; however, this geometry prevents any conjugation between these groups that helps stabilize the final Mpa product.

Another direct pathway for producing Mpa starts at the bidentate Li^+(Cys) [CO,S] ttgt intermediate, the second intermediate shown in Figure 6. This conformer binds the lithium cation in a position that matches that of ground state Li^+(Mpa) [CO,S] ttct with the amino group remote from the lithium site. A transition state in which a hydrogen atom on C_β is transferred directly to the amino group was located and found to lie 276−301 kJ/mol above the reactant GS (122−144 kJ/mol above TS[NH_3 loss]).

We next explored several pathways in which one of the thiirane-containing intermediates formed in Figure 6 could rearrange to an intermediate having one of the alternate $C_3H_4O_2S$ isomers. For instance, from $(NH_3)Li^+$(Tica) [CO,S] tg, a 1,2-hydrogen shift from C_β to S would lead directly to $(NH_3)Li^+$(Mpa) [CO,S] ttct. A TS for this transformation was located 206−275 kJ/mol above the Li^+(Cys) GS reactant (59−118 kJ/mol above TS[NH_3 loss]). Alternatively, from $(NH_3)Li^+$(Tica) [CO_2^-] cc, a synchronous motion that breaks the C−S bond and transfers a hydrogen from C_β to the carboxylic acid group leads to formation of $(NH_3)Li^+$(Mpa) [CO] ccct. This involves a TS lying 238−271 kJ/mol above the Li^+(Cys) GS reactant (91−114 kJ/mol above TS[NH_3 loss]). Finally, we located a TS that interchanged $(NH_3)Li^+$(Mpa) [CO,S] ttct with $(NH_3)Li^+$(Taca) [CO,S] ttc at 161−202 kJ/mol above the reactant GS (15−45 kJ/mol above TS[NH_3 loss]), although this TS still does not provide a viable pathway to form either of these species from the $(NH_3)Li^+$(Tica) isomer. There may be other pathways that could form the alternate $C_3H_4O_2S$ isomers, but the pathways explored here illustrate that these are all likely to be high in energy, >59 kJ/mol above the rate-limiting transition state shown in Figure 6.

4. Discussion

Experimental Thermochemistry. From the competitive modeling of the Li^+(Cys) data shown in Figure 2, which includes reactions 3a, 3b, and 4, we obtain bond energies for Li^+-Cys as well as the barrier for deamination. These are listed in Table 6 along with bond energies for $Li^+(C_3H_4O_2S)-NH_3$ and $Li^+(NH_3)-C_3H_4O_2S$ obtained experimentally from a competitive analysis of the data for decomposition of the $(NH_3)Li^+$-$(C_3H_4O_2S)$ isomer, as shown in Figure 3. In addition, the difference in the latter two bond energies must equal the difference in the bond energies for $Li^+-C_3H_4O_2S$ and Li^+-NH_3, such that a value for $D_0(Li^+-C_3H_4O_2S)$ can be derived by combining this difference, 0.62 ± 0.07 eV, with $D_0(Li^+-NH_3)$ from the literature, 159.1 ± 10.3 kJ/mol.[41,58,59] This threshold difference leads to $D_0(Li^+-C_3H_4O_2S)$ = 219.1 ± 12.1 kJ/mol. Likewise, a second somewhat independent measure of $D_0(Li^+-C_3H_4O_2S)$ comes from the difference in thresholds for formation of $Li^+(C_3H_4O_2S)$ and Li^+, 2.35 ± 0.09 eV or 226.3 ± 8.6 kJ/mol, a value in good agreement with the first approach. The validity of the thermochemistry can be assessed by comparison of the literature value for $D_0(Li^+-NH_3)$, 159.1 ± 10.3 kJ/mol, with the difference in the thresholds for formation of $Li^+(NH_3)$ and Li^+, 1.72 ± 0.09 eV or 166.3 ± 9.0 kJ/mol. The agreement in these two values illustrates the self-consistency of the relative thresholds measured here. The weighted average of the two values for $D_0(Li^+-C_3H_4O_2S)$ determined here, 223.9 ± 14.0 kJ/mol, is taken as our best value, where the uncertainty is two standard deviations of the mean.

To this point, the only threshold listed in Table 1 that has not been used to derive thermodynamic information is that listed for reaction 3b, the formation of $Li^+ + C_3H_4O_2S + NH_3$ from Li^+(Cys) obtained from the model including reactions 3a, 3b, and 4. Combined with the threshold for $Li^+ +$ Cys, reaction 3a, this threshold should give an experimental measure of the relative heats of formation of Cys and its $C_3H_4O_2S + NH_3$ fragments, 1.19 ± 0.30 eV. Combined with the threshold for

TABLE 6: Experimental and Theoretical Binding Energies (kJ/mol) at 0 K for Lithiated Complexes

			theory[a]		
bond	experiment	structure	B3LYP	B3P86	MP2(full)
Li^+-Cys	255.8 ± 11.9	[N,CO,S]tggg$_+$	260.0*	251.1*	258.0 (245.7*)
			263.8	*254.3*	*255.6*
Li^+-NH_3	159.1 ± 10.3[b]		158.1*	154.5*	155.0 (150.6*)
			161.1	*157.5*	*156.0*
$Li^+(C_3H_4O_2S)-NH_3$	109.0 ± 4.1	Tica [CO,S]tg	113.7	111.2	119.8
			110.3	*108.6*	*117.8*
		Taca [CO,S]ttc	109.0	106.8	116.5
		Mpa [CO,S]ttct	114.0	112.9	119.4
		Mpa [CO]tctc	123.2	119.2	126.2
$Li^+(NH_3)-C_3H_4O_2S$	169.0 ± 6.2	Tica [CO,S]tg	167.2	163.1	169.5
			166.2	*162.3*	*168.8*
		Taca [CO,S]ttc	170.3	165.6	168.5
		Mpa [CO,S]ttct	155.5	149.3	154.1
		Mpa [CO]tctc	165.8	159.5	155.9
$Li^+-C_3H_4O_2S$	223.9 ± 14.0	Tica [CO,S]tg	211.0*	205.9*	204.8 (195.0*)
			212.9	*207.6*	*204.5*
		Taca [CO,S]ttc	218.9*	212.7*	207.0 (196.5*)
			222.4	*216.3*	*208.5*
		Mpa [CO,S]ttct	199.0*	190.3*	189.7 (180.0*)
			202.6	*194.0*	*191.3*
		Mpa [CO]tctc	200.8*	194.8*	184.8 (178.0*)
			205.5	*199.0*	*187.4*
$Li^+(Cys)-NH_3$ (TS)	166.0 ± 16.9		143.0	151.7	156.9
			139.2	*145.3*	*144.5*
MAD[c]			7.9	8.3	7.6 (11.3)
			8.6	*6.8*	*8.9*

[a] All structures geometry optimized and have zero point energy corrections calculated at the B3LYP/6-311G(d,p) level. Final energies are taken from single point energies calculated at the levels indicated using 6-311+G(2d,2p) basis sets. Values in italics have geometries optimized and zero point energies calculated at the MP2(full)/cc-pVDZ(Li−C) level with single point energies calculated at the levels indicated using the aug-cc-pVTZ(Li−C) basis set. Values that include counterpoise (cp) corrections are noted by an asterisk. [b] Value from refs 41, 58, and 59. [c] Mean absolute deviation from all six experimental values for energies calculated assuming the Tica fragment.

$Li^+ + C_3H_4O_2S + NH_3$ from $(NH_3)Li^+(C_3H_4O_2S)$, this same threshold gives the relative energies of the Li^+(Cys) and $(NH_3)Li^+(C_3H_4O_2S)$ complexes, 0.37 ± 0.29 eV. However, the threshold for reaction 3b is the least reliable measurement here because this onset is masked by the lower energy formation of the same product ion in reaction 3a and because the application of the statistical sequential dissociation model is not rigorously correct.

Comparison of Theoretical and Experimental Thermochemistry: Products. Table 6 compares the experimental bond energies derived here with values calculated theoretically. It can be seen that agreement for Li^+(Cys) and $Li^+(NH_3)$ is very good, with all theoretical values lying well within the experimental uncertainties, although MP2(full) values with counterpoise corrections are low.

Three of the bond energies in Table 6 involve the $C_3H_4O_2S$ fragment, for which there are several possibilities. Given the good agreement between experiment and this level of theory for Li^+(Cys) and $Li^+(NH_3)$, as well as many other ligands,[41] which of the various possible $C_3H_4O_2S$ fragments might be formed in these decomposition reactions can be identified by comparison of these bond energies with theory. As noted above, the experimental thresholds obtained are insensitive to which isomer is assumed when analyzing these data, varying by less than 8 kJ/mol. Further, the theoretical bond energies listed in Table 6 presume that the $C_3H_4O_2S$ ligand does not convert between the different isomers upon dissociation, which seems reasonable given that calculations of the barriers for such isomerizations confirm that they are fairly high in energy, as discussed above. The experimental value for $D_0(Li^+-C_3H_4O_2S)$ is in agreement with theory for either the Tica or Taca isomers, with the aug-cc-PVTZ(Li−C) and B3LYP results providing better agreement than other approaches. In contrast, the calculated bond energies for the Mpa isomer are too low at all levels of theory. Furthermore, the theoretical values for the $Li^+(C_3H_4O_2S)-NH_3$ and $Li^+(NH_3)-C_3H_4O_2S$ bond energies agree nicely with the directly measured thresholds, which confirms the hypothesis that the bis-ligated $(NH_3)Li^+(C_3H_4O_2S)$ complex is generated in the flow tube source along with varying amounts of Li^+(Cys). Note that the energy for losing ammonia is relatively insensitive to the identity of the $C_3H_4O_2S$ isomer, with values for different isomers at a specific level of theory agreeing within 9 kJ/mol, except for the Li^+(Mpa) [CO] tctc isomer, where the calculated value is another 6−9 kJ/mol higher and outside of experimental uncertainty. The threshold measured for formation of $Li^+(NH_3) + C_3H_4O_2S$ agrees well with theory if the $C_3H_4O_2S$ isomer is Tica or Taca, whereas that for Mpa-tctc is somewhat low (except for the B3LYP value), and that for Mpa-ttct is outside experimental uncertainty. These comparisons suggest that the isomer of $C_3H_4O_2S$ generated is Tica or Taca but unlikely to be Mpa. Likewise, the Mpl isomer is excluded on the basis of its very high energy, Tables 2 and 3.

We can also compare the relative thermochemistry derived from the threshold for reaction 3b: Cys versus $C_3H_4O_2S + NH_3$ and Li^+(Cys) versus $(NH_3)Li^+(C_3H_4O_2S)$. In the former case, the experimental threshold difference corresponds to the fragments having a heat of formation higher than Cys by 115 ± 29 kJ/mol. This is considerably higher than calculated values for Cys versus Mpa-ttcc (5−39 kJ/mol), Mpa-tctc (12−47 kJ/mol), Taca-ttt (37−64 kJ/mol), or Tica-tt (43−56 kJ/mol). Likewise, the experimental threshold for reaction 3b suggests that $(NH_3)Li^+(C_3H_4O_2S)$ lies higher in energy than Li^+(Cys) by 36

± 28 kJ/mol, compared to theoretical differences listed in Table 4 that are negative for the ground state conformers of each type of $C_3H_4O_2S$ isomer. These discrepancies may simply be because the application of the statistical sequential dissociation model to this system is not rigorously correct; however, the sign of the discrepancies suggests that, because the loss of ammonia in reaction 4 passes over a tight transition state, the NH_3 can carry away more energy than is predicted by the sequential dissociation model, such that subsequent dissociation of the $Li^+(C_3H_4O_2S)$ product in reaction 3b is delayed to higher energies. As a consequence, we believe that the "threshold" for reaction 3b obtained from the competitive modeling including reactions 3a, 3b, and 4 can only be viewed as an upper limit to the true thermodynamic threshold, such that the thermochemistry derived from this threshold provides relative energy differences that are too large. Further support for this hypothesis comes from a comparison of the branching ratios of the $Li^+(C_3H_4O_2S)$ and $Li^+(NH_3)$ products in Figures 2 and 3. In Figure 3, the successful modeling of all three channels and their self-consistent thermochemistry demonstrates that the dissociation of the $(NH_3)Li^+(C_3H_4O_2S)$ complex is statistically behaved. Compared to Figure 3, the amount of $Li^+(NH_3)$ formed relative to $Li^+(C_3H_4O_2S)$ is smaller even though the relative threshold is lower, consistent with different dynamics in this system once past the tight TS.

Comparison of Theoretical and Experimental Thermochemistry: Transition State. We compare our measured thresholds for ammonia loss from Li^+(Cys) in reaction 4 to theoretical calculations for the lowest energy rate-limiting TS in Table 6. Theory finds that the transition state for NH_3 elimination, TS[NH_3 loss], lies 139−157 kJ/mol above the Li^+(Cys) ground reactant complex. These calculated energies are slightly lower than our measured threshold of 166.0 ± 16.9 kJ/mol (taken from the competitive model including reactions 3a, 3b, and 4) but within experimental uncertainty. Of the alternative TSs located, the next lowest has an energy of 206−275 kJ/mol, well above the experimental value.

We also considered the possibility that the threshold observed for reaction 4 should have been analyzed assuming a loose PSL TS. Such an assumption would increase the measured threshold appreciably because the looser TS would reduce the kinetic shift associated with the tight TS. However, for such an assumption to be appropriate, the derived threshold value would then correspond to the energy of the $Li^+(C_3H_4O_2S) + NH_3$ asymptote, which is calculated to lie at 93−107 kJ/mol for Li^+(Tica) [CO,S]tg, 67−120 kJ/mol for the two low- energy Li^+(Mpa) isomers, and 79−113 kJ/mol for Li^+(Taca) [CO,S] ttc. Thus, the assumption of a loose TS for reaction 4 leads to a discrepancy with experiment of >50 kJ/mol. Furthermore, use of a loose TS for reaction 4 would not be consistent with the extent of competition observed experimentally between this process and reaction 3a, Figure 2.

The differences between the experimental and theoretical energies for the tight TS parallel those observed in a previous study of the decompositions of Li^+(Ser) and Li^+(Thr).[49] There, we found that theoretical energies of five transition states calculated at the MP2(full) level were in particularly good agreement with experiment, with a mean absolute deviation (MAD) of 5 ± 5 kJ/mol, well within experimental uncertainty. In contrast, density functional theory (DFT) calculations were systematically lower than the experimental values by 34 ± 5 (B3LYP) and 24 ± 5 (B3P86) kJ/mol, about 10 kJ/mol larger than the discrepancies observed here. These large differences in accuracy contrast with the behavior for the noncovalent bond energies of these and many other systems where the DFT results are much closer to the MP2(full) and experimental results.[41,52,60]

Overall, the agreement between the experimental threshold for reaction 4 and theoretical values for TS[NH_3 loss] affirms that the product formed in the deamination of cysteine is the thiirane-carboxylic acid (Tica). As noted above, this assignment is also consistent with the bond energies obtained for NH_3-Li^+(Tica), $(NH_3)Li^+-$Tica, and Li^+-Tica. Mean absolute deviations (MADs) between experiment and theory for all of the thermochemistry data provided in Table 6 are less than 9 kJ/mol for all levels of theory.

Conclusion

In addition to loss of the intact amino acid, elimination of ammonia is observed in the collision-induced dissociation of Li^+(Cys). This decomposition is also observed to occur in the source region generating the isobaric $(NH_3)Li^+(C_3H_4O_2S)$ complex. Analysis of the experimental data requires that competition among the various products be accounted for in order to provide accurate thermochemistry. Modeling of the kinetic energy dependences of the decompositions of both complexes allows the extraction of the bond energy of lithium cations to cysteine, as well as values for NH_3-Li^+(Tica), $(NH_3)Li^+-$Tica, Li^+-Tica, and Li^+-NH_3, where the latter agrees with the literature.[41,58,59] Finally, the threshold observed for reaction 4 is also obtained and corresponds to a barrier along the potential energy surface for deamination of lithiated cysteine.

Extensive quantum chemical calculations are performed to investigate the possible mechanisms for NH_3 elimination from Li^+(Cys). The lowest energy pathway located for NH_3 loss involves hydrogen transfer from the carboxylic acid group to the amino group followed by backside attack of the thio group at the α carbon to induce cleavage of the C−N bond. The calculated rate-limiting tight TS has an MP2(full)/6-311+G(2d,2p)//B3LYP/6-311G(d,p) energy in good agreement with the experimental threshold for this reaction. The calculated reaction pathways identify that the $C_3H_4O_2S$ product formed in this reaction is likely to be the thiirane-carboxylic acid (Tica). Theoretical investigations of the isomers of $C_3H_4O_2S$, $Li^+(C_3H_4O_2S)$, and $(NH_3)Li^+(C_3H_4O_2S)$ are also conducted. The experimental BDEs for loss of NH_3 and $C_3H_4O_2S$ from the latter complex and for $Li^+-C_3H_4O_2S$ agree well with calculated values for the Taca and Tica isomers but not with Mpa isomers. Overall, the comparison of experiment and theory identifies the reaction pathway for deamination of Li^+(Cys) and allows the conclusion that the $(C_3H_4O_2S)$ fragment is Tica.

Acknowledgment. This work is supported by the National Science Foundation, grant CHE-0748790. A grant of computer time from the Center for High Performance Computing at the University of Utah is gratefully acknowledged.

Supporting Information Available: Figure showing the various transition states for deamination described in the text. This material is available free of charge via the Internet at http://pubs.acs.org.

References and Notes

(1) Armentrout, P. B.; Armentrout, E. I.; Clark, A. A.; Cooper, T. E.; Stennett, E. M. S.; Carl, D. R. *J. Phys. Chem. B*. DOI: 10.1021/jp911219u.

(2) Cody, R. B.; Amster, I. J.; McLafferty, F. W. *Proc. Natl. Acad. Sci. U.S.A.* **1985**, *82*, 6367.

(3) Renner, D.; Spiteller, G. *Biomed. Environ. Mass Spectrom.* **1988**, *15*, 75.

(4) Tang, X.; Ens, W.; Standing, K. G.; Westmore, J. B. *Anal. Chem.* **1988**, *60*, 1791.

(5) Russell, D. H.; McGlohon, E. S.; Mallis, L. M. *Anal. Chem.* **1988**, *60*, 1818.
(6) Grese, R. P.; Cerny, R. L.; Gross, M. L. *J. Am. Chem. Soc.* **1989**, *111*, 2835.
(7) Grese, R. P.; Gross, M. L. *J. Am. Chem. Soc.* **1990**, *112*, 5098.
(8) Leary, J. A.; Zhou, Z.; Ogden, S. A.; Williams, T. D. *J. Am. Soc. Mass Spectrom.* **1990**, *1*, 473.
(9) Kish, M. M.; Wesdemiotis, C. *Int. J. Mass Spectrom.* **2003**, *227*, 191.
(10) Ervin, K. M.; Armentrout, P. B. *J. Chem. Phys.* **1985**, *83*, 166.
(11) Muntean, F.; Armentrout, P. B. *J. Chem. Phys.* **2001**, *115*, 1213.
(12) Schultz, R. H.; Crellin, K. C.; Armentrout, P. B. *J. Am. Chem. Soc.* **1991**, *113*, 8590.
(13) Fisher, E. R.; Armentrout, P. B. *J. Chem. Phys.* **1991**, *94*, 1150.
(14) Fisher, E. R.; Kickel, B. L.; Armentrout, P. B. *J. Chem. Phys.* **1992**, *97*, 4859.
(15) Rodgers, M. T.; Armentrout, P. B. *J. Phys. Chem. A* **1997**, *101*, 1238.
(16) Rodgers, M. T.; Armentrout, P. B. *Int. J. Mass Spectrom.* **1999**, *185/186/187*, 359.
(17) Rodgers, M. T.; Armentrout, P. B. *J. Phys. Chem. A* **1999**, *103*, 4955.
(18) Moision, R. M.; Armentrout, P. B. *Phys. Chem. Chem. Phys.* **2004**, *6*, 2588.
(19) Moision, R. M.; Armentrout, P. B. *J. Phys. Chem. A* **2006**, *110*, 3933.
(20) Rodgers, M. T.; Ervin, K. M.; Armentrout, P. B. *J. Chem. Phys.* **1997**, *106*, 4499.
(21) Rodgers, M. T.; Armentrout, P. B. *J. Chem. Phys.* **1998**, *109*, 1787.
(22) Beyer, T. S.; Swinehart, D. F. *Commun. Assoc. Comput. Mach.* **1973**, *16*, 379.
(23) Gilbert, R. G.; Smith, S. C. *Theory of Unimolecular and Recombination Reactions*; Blackwell Scientific: London, 1990.
(24) Truhlar, D. G.; Garrett, B. C.; Klippenstein, S. J. *J. Phys. Chem.* **1996**, *100*, 12771.
(25) Holbrook, K. A. Pilling, M. J. Robertson, S. H. *Unimolecular Reactions*, 2nd ed.; Wiley: New York, 1996.
(26) Moision, R. M.; Armentrout, P. B. *J. Phys. Chem. A* **2002**, *106*, 10350.
(27) Meyer, F.; Khan, F. A.; Armentrout, P. B. *J. Am. Chem. Soc.* **1995**, *117*, 9740.
(28) Koizumi, H.; Armentrout, P. B. *J. Am. Soc. Mass Spectrom.* **2001**, *12*, 480.
(29) Ye, S. J.; Moision, R. M.; Armentrout, P. B. *Int. J. Mass Spectrom.* **2006**, *253*, 288.
(30) More, M. B.; Ray, D.; Armentrout, P. B. *J. Phys. Chem. A* **1997**, *101*, 831.
(31) More, M. B.; Ray, D.; Armentrout, P. B. *J. Phys. Chem. A* **1997**, *101*, 4254.
(32) More, M. B.; Ray, D.; Armentrout, P. B. *J. Phys. Chem. A* **1997**, *101*, 7007.
(33) Ye, S. J.; Armentrout, P. B. *J. Phys. Chem. A* **2008**, *112*, 3587.
(34) Armentrout, P. B. *J. Chem. Phys.* **2007**, *126*, 234302.
(35) Frisch, M. J.; Trucks, G. W.; Schlegel, H. B.; Scuseria, G. E.; Robb, M. A.; Cheeseman, J. R.; Montgomery, J. A., Jr.; Vreven, T.; Kudin, K. N.; Burant, J. C.; Millam, J. M.; Iyengar, S. S.; Tomasi, J.; Barone, V.; Mennucci, B.; Cossi, M.; Scalmani, G.; Rega, N.; Petersson, G. A.; Nakatsuji, H.; Hada, M.; Ehara, M.; Toyota, K.; Fukuda, R.; Hasegawa, J.; Ishida, M.; Nakajima, T.; Honda, Y.; Kitao, O.; Nakai, H.; Klene, M.; Li, X.; Knox, J. E.; Hratchian, H. P.; Cross, J. B.; Adamo, C.; Jaramillo, J.; Gomperts, R.; Stratmann, R. E.; Yazyev, O.; Austin, A. J.; Cammi, R.; Pomelli, C.; Ochterski, J. W.; Ayala, P. Y.; Morokuma, K.; Voth, G. A.; Salvador, P.; Dannenberg, J. J.; Zakrzewski, V. G.; Dapprich, S.; Daniels, A. D.; Strain, M. C.; Farkas, O.; Malick, D. K.; Rabuck, A. D.; Raghavachari, K.; Foresman, J. B.; Ortiz, J. V.; Cui, Q.; Baboul, A. G.; Clifford, S.; Cioslowski, J.; Stefanov, B. B.; Liu, G.; Liashenko, A.; Piskorz, P.; Komaromi, I.; Martin, R. L.; Fox, D. J.; Keith, T.; Al-Laham, M. A.; Peng, C. Y.; Nanayakkara, A.; Challacombe, M.; Gill, P. M. W.; Johnson, B.; Chen, W.; Wong, M. W.; Gonzalez, C.; Pople, J. A. *Gaussian 03*; Gaussian, Inc.: Pittsburgh, PA, 2003.
(36) McLean, A. D.; Chandler, G. S. *J. Chem. Phys.* **1980**, *72*, 5639.
(37) Krishnan, R.; Binkley, J. S.; Seeger, R.; Pople, J. A. *J. Chem. Phys.* **1980**, *72*, 650.
(38) Foresman, J. B.; Frisch, A. E. *Exploring Chemistry with Electronic Structure Methods*, 2nd ed.; Gaussian, Inc.: Pittsburgh, PA, 1996.
(39) Boys, S. F.; Bernardi, R. *Mol. Phys.* **1970**, *19*, 553.
(40) van Duijneveldt, F. B.; van Duijneveldt de Rijdt, J. G. C. M.; van Lenthe, J. H. *Chem. Rev.* **1994**, *94*, 1873.
(41) Rodgers, M. T.; Armentrout, P. B. *Int. J. Mass Spectrom.* **2007**, *267*, 167.
(42) Woon, D. E.; Dunning, T. H. *J. Chem. Phys.* **1995**, *103*, 4572.
(43) Dunning, T. H. *J. Chem. Phys.* **1989**, *90*, 1007.
(44) Kendall, R. A.; Dunning, T. H.; Harrison, R. J. *J. Chem. Phys.* **1992**, *96*, 6796.
(45) Dookeran, N. N.; Yalcin, T.; Harrison, A. G. *J. Mass Spectrom.* **1996**, *31*, 500.
(46) Klassen, J. S.; Kebarle, P. *J. Am. Chem. Soc.* **1997**, *119*, 6552.
(47) O'Hair, R. A. J.; Broughton, P. S.; Styles, M. L.; Frink, B. T.; Hadad, C. M. *J. Am. Soc. Mass Spectrom.* **2000**, *11*, 687.
(48) Rogalewicz, F.; Hoppilliard, Y.; Ohanessian, G. *Int. J. Mass Spectrom.* **2000**, *195/196*, 565.
(49) Ye, S. J.; Armentrout, P. B. *J. Phys. Chem. B* **2008**, *112*, 10303.
(50) Heaton, A. L.; Ye, S. J.; Armentrout, P. B. *J. Phys. Chem. A* **2008**, *112*, 3328.
(51) Heaton, A. L.; Armentrout, P. B. *J. Am. Soc. Mass Spectrom.* **2009**, *20*, 852.
(52) Ye, S. J.; Clark, A. A.; Armentrout, P. B. *J. Phys. Chem. B* **2008**, *112*, 10291.
(53) Armentrout, P. B.; Gabriel, A.; Moision, R. M. *Int. J. Mass Spectrom.* **2009**, *283*, 56.
(54) Ye, S. J.; Moision, R. M.; Armentrout, P. B. *Int. J. Mass Spectrom.* **2005**, *240*, 233.
(55) O'Hair, R. A. J.; Styles, M. L.; Reid, G. E. *J. Am. Soc. Mass Spectrom.* **1998**, *9*, 1275.
(56) Baldwin, J. E. *J. Chem. Soc., Chem. Commun.* **1976**, 734.
(57) Baldwin, J. E.; Thomas, R. C.; Kruse, L. I.; Silberman, L. *J. Org. Chem.* **1977**, *42*, 3846.
(58) Taft, R. W.; Anvia, F.; Gal, J.-F.; Walsh, S.; Capon, M.; Holmes, M. C.; Hosn, K.; Oloumi, G.; Vasanwala, R.; Yazdani, S. *Pure Appl. Chem.* **1990**, *62*, 17.
(59) Burk, P.; Koppel, I. A.; Koppel, I.; Kurg, R.; Gal, J.-F.; Maria, P.-C.; Herreros, M.; Notario, R.; Abboud, J.-L. M.; Anvia, F.; Taft, R. W. *J. Phys. Chem. A* **2000**, *104*, 2824.
(60) Armentrout, P. B.; Rodgers, M. T. *J. Phys. Chem. A* **2000**, *104*, 2238.

JP911222J